JACS
JOURNAL OF THE AMERICAN CHEMICAL SOCIETY
Article
pubs.acs.org/JACS

Femtosecond Electron Solvation at the Ionic Liquid/Metal Electrode Interface

Eric A. Muller,[†,‡] Matthew L. Strader,[‡] James E. Johns,[§] Aram Yang,[†] Benjamin W. Caplins,[†,‡] Alex J. Shearer,[†,‡] David E. Suich,[†,‡] and Charles B. Harris*[,†,‡]

[†]Department of Chemistry, University of California at Berkeley, Berkeley, California, United States
[‡]Chemical Sciences Division, Lawrence Berkeley National Laboratory, Berkeley, California 94720, United States
[§]Department of Materials Science and Engineering and Medicine, Northwestern University, Evanston, Illinois 60208, United States

ABSTRACT: Electron solvation is examined at the interface of a room temperature ionic liquid (RTIL) and an Ag(111) electrode. Femtosecond two-photon photoemission spectroscopy is used to inject an electron into an ultrathin film of RTIL 1-butyl-1-methylpyrrolidinium bis(trifluoromethylsulfonyl)-imide ($[Bmpyr]^+[NTf_2]^-$). While much of current literature highlights slower nanosecond solvation mechanisms in bulk ionic liquids, we observe only a femtosecond response, supporting morphology dependent and interface specific electron solvation mechanisms. The injected excess electron is found to reside in an electron affinity level residing near the metal surface. Population of this state decays back to the metal with a time constant of 400 ± 150 fs. Electron solvation is measured as a dynamic decrease in the energy with a time constant of 350 ± 150 fs. We observe two distinct temperature regimes, with a critical temperature near 250 K. The low temperature regime is characterized by a higher work function of 4.41 eV, while the high temperature regime is characterized by a lower work function of 4.19 eV. The total reorganizational energy of solvation changes above and below the critical temperature. In the high temperature regime, the electron affinity level solvates by 540 meV at 350 K, and below the critical temperature, solvation decreases to 200 meV at 130 K. This study will provide valuable insight to interface specific solvation of room temperature ionic liquids.

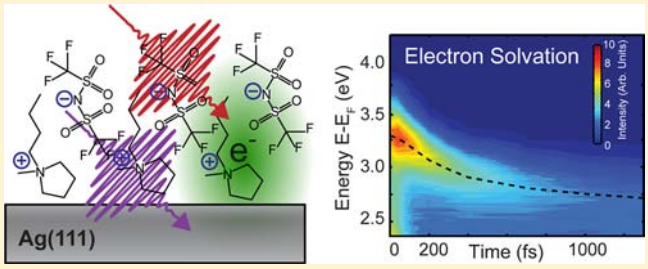

1. INTRODUCTION AND BACKGROUND

Room temperature ionic liquids (RTILs) constitute a unique solvent class consisting of charge separated ions, providing electrical conductivity without the need for solute ions. RTILs have found increasing application in "green" industrial solvents[1] and as solvents for heterogeneous catalysis.[2] Ionic conductivity, stability, and low volatility have encouraged applications in Gratzel cells[3] and Li^+ ion batteries.[4,5] Ionic conductivity and ion transport are known to be critically linked to electron solvation kinetics.[6] Viscosity is proposed as a kinetic barrier to bulk charge transport[7] and has prevented commercial implementation of devices relying on bulk conductivity,[8,9] though devices that rely only upon interfacial solvent response may experience faster solvation kinetics.[10] We present here an investigation of electron solvation within ultrathin films of RTIL/Ag(111), using time- and angle-resolved two-photon photoemission spectroscopy (TPPE). Our findings are of general interest to a molecular and mechanistic understanding of charge injection and solvation and are directly relevant toward electrochemical applications of RTILs.

A significant amount of research has been performed with the goal of a molecular understanding of solvation kinetics in RTILs. Solvation in RTILs may be expected to be unique from other solvents and highly dependent upon anion and cation chemical identity, local ordering, and details of the solute. Much of the current knowledge of solvation in RTILs has been based upon spectroscopic investigations of bulk solvent, using optically excited dye molecules as probes of solvent kinetics or Kerr effect spectroscopy to measure intermolecular dynamics in neat ionic liquids.[11,12] Solvent response functions often span 10^{-13}–10^{-8} s within a single solute–solvent system.[13,14] In general, solvation of an excited state solute can be qualitatively understood through a dielectric continuum description as the frequency dependent dielectric response of the bulk solvent, though this typically underestimates solvation times.[14]

Several studies have found that solvation of a solute in bulk RTIL has two main components, an ultrafast subpicosecond time scale and a slower component on nanosecond time scale. Components of the biexponential behavior have been attributed to system dependent anion–cation interactions.[15] In other cases, the fast component has been attributed to cation polarizability while the slow component is attributed to diffusional motion of the anion.[16] Biexponential kinetics have also been attributed to microscopic or nanoscopic domain formation.[17] Homophilicity of both the alkane ligands and the aromatic ionic cores results in the formation of heterogeneous domains. High local concentrations of either the ionic or

Received: November 4, 2012
Published: June 21, 2013

   dx.doi.org/10.1021/ja3108593 | J. Am. Chem. Soc. 2013, 135, 10646–10653

hydrophobic moieties give rise to two dramatically different solvation times in which the alkane rich regions solvate at a dramatically different rate than the ionic regions.[18] Recent studies examining the solvation times of charged and neutral solutes within a given ionic liquid show different amplitudes of the fast and slow components of reorganizational energy or orientational diffusion,[19,20] depending upon the relative solubility (and thus concentration) of the solute in the ionic versus hydrophobic domains.

Bulk solvation studies are complicated by glassy dynamics and hindered solvent motion near the critical temperature. Hindered motions result in complex relaxation kinetics containing multiexponential or stretched-exponential components.[15,16,21]

The dynamics of ultrafast solvation of excess electrons has been recently investigated, removing dependence of solvation dynamics on the solute structure and more directly probing the dynamics of the RTILs themselves. Excess electrons, produced by incident high energy (UV or X-ray) photons, are found to localize on one or a few solvent ions.[22] Similar to the response found in excited dye solutes, the electrons are found to solvate on multiple time scales.[23] The localization site and the resulting chemical environment experienced by the solvated electron remain a hotly debated topic, and theoretical work has proposed that the electron can localize on either the cation or the anion depending upon the relative electron affinity levels of the two species.[24]

Molecular ordering and morphology of RTILs at interfaces, however, differ greatly from the bulk morphology. The RTIL/air and RTIL/vacuum interfaces contain highly ordered layers of alternating cations and anions for the first few layers, as observed in both theory[25] and experiment.[26] The image force is found to play a strong role here; ionic charges are *repelled* from the vacuum interface as a result of the lower dielectric constant.[27] As a result, alkyl chains, which are generally found on the cation, form a nonpolar layer at the vacuum interface.[28]

Ordered layers form at the interface of RTIL and a solid substrate, and substrate specific forces are found to play an important role. For example, the image force plays an opposite role at the RTIL/substrate interface compared to the RTIL/vacuum interface: at the interface with a high dielectric substrate, the image force *attracts* charged ionic species. The image force is in competition with the substrate surface charge, which may be polar or nonpolar, the polarizability of the substrate, and the potential for chemical bonding. Addition of a net charge to the substrate surface via an applied voltage directly alters the ordering of a RTIL layer.[29−31]

Several techniques have been used to directly probe this layered ordering. Scanning tunneling microscopy (STM) and atomic force microscopy (AFM) investigations have found ordered molecular layers of alternating cations and anions out to >5 molecular layers (ML),[30,32−34] though this may be influenced by the presence of the probe tip. Photoelectron spectroscopy has revealed the growth modes of several ionic liquids.[35−37] Ionic liquids at the electrode interface are found to organize with layers of alternating cations and anions[29] or in mixed "checkerboard" bilayers.[37] In the case of dialkylpyrrolidinium bis(trifluoromethylsulfonyl) ionic liquids, the length of the alkyl chain has been found to play an important role driving organization at a mica substrate.[38] Short alkyl chains result in alternating layers of cations and anions, whereas longer alkyl chains transition to a checkerboard bilayer growth mode. In general, the complex interactions at the surface result in increased ordering, which differs dramatically from the bulk.

Electron solvation kinetics and mechanisms are fundamentally dependent upon molecular ordering, mobility, and the dimensionality of the system. Recent experimental and theoretical studies have found interface-specific solvation mechanisms. A recent experimental study of the temperature-dependent capacitive response of a pyrrolidinium ionic liquid/Au(111) found both an Arrhenius activated fast response and a temperature-independent slow response.[39] A recent theoretical study found that the interfacial capacitance of the molecule/substrate interface is dominated (>80%) by a femtosecond solvation response,[40] followed by a smaller slow response. This contrasts with solvation in bulk liquids, which typically finds the nanosecond response to be dominant. Interface-specific solvation mechanisms remain an emerging area of study, however, lacking general chemical trends.

TPPE is well suited for obtaining a molecular understanding of electron solvation mechanisms at the solvent−electrode interface. This technique measures the dynamic response to a photo-injected electron while being sensitive to the chemical environment and molecular ordering at the interface. This technique has been applied extensively toward understanding both polar and nonpolar solvents at the solvent/vacuum and solvent/electrode interfaces.

In particular, detailed TPPE investigations in thin films of ice (H_2O or D_2O) on Ru(001) and Cu(111) highlight the utility of this technique and the importance of morphology. Here, electrons are photoinjected into an image potential state (IPS) or conduction band state (CB), which are found to be initially delocalized, with effective mass near that of a free electron. The photoinjected electronic state (e_s) solvates on a time scale of typically a few hundred femtoseconds. Solvation of e_s is observed directly as an energetic stabilization relative to the Fermi level, often with an associated increase in barrier to decay back to the metal substrate.[41] In D_2O/Cu(111), this is accompanied by a decrease in the spatial extent of excited state electrons, from 20 to 10 Å within 1.3 ps.[42] Morphology plays an important role in these systems,[43] and electrons are found to localize more rapidly in amorphous films than crystalline because of the high density of defect states, and solvation in island clusters has been found to occur at edge states.[44] Solvation at amorphous defect sites and island edges is attributed to decreased hydrogen-bonding order and resulting increased mobility.[41] In contrast, directional binding of monolayer H_2O/TiO_2 inhibits solvation, as observed by ultrafast (<15 fs) decay times.[45]

Electron solvation kinetics are highly dependent upon molecule substrate binding, the exact identity of the electronic state, and the solvation mechanism. In methanol/TiO_2, an initially localized conduction band electron solvates on the femtosecond time scale.[46] Solvation is mediated by motion of the alcohol group, and kinetics are heavily dependent upon isotopic substitution.[47] In methanol/Ag(111), however, apparent solvation of a delocalized image state results from a rotation of the molecular dipole moment and change in the local work function.[48] As a result, solvation occurs homogenously across the image state progression, and no evidence of substantial isotope effect or localization is observed. Similarly, in a one monolayer (1 ML) coverage of dimethylsulfoxide/Ag(111), strong and directional Ag−S substrate binding hinders rotation of the molecular dipole and prevents solvation of the IPS.[49] In multilayer coverages, however, adsorbed

dx.doi.org/10.1021/ja3108593 | J. Am. Chem. Soc. 2013, 135, 10646−10653

molecules are free to rotate, and solvation by >200 meV accompanies an ultrafast localization of the image potential state.

In this work, we apply TPPE to the study of electron solvation in ultrathin films of 1-butyl-1-methylpyrrolidinium bis(trifluoromethylsulfonyl)imide ($[Bmpyr]^+[NTf_2]^-$)/Ag-(111). Our results draw together investigations of bulk solvation in RTIL, RTIL surface structure, and TPPE investigations of interfacial solvation dynamics in conventional solvents. The low vapor pressures of RTIL allow investigations in ultrahigh vacuum at temperatures near ambient conditions, which is not possible for common dipolar or nonpolar organic solvents. We investigate electron solvation of an electron affinity (EA) level through its band structure, population dynamics, solvation dynamics, and temperature dependence. Our results show new, interface-specific electron solvation mechanisms. We expect qualitative findings of ultrafast electron solvation to be general across RTILs, though specific rates and mechanisms are likely system specific, meriting further detailed study.

2. EXPERIMENTAL SECTION

An atomically clean Ag(111) substrate was prepared under ultrahigh vacuum conditions by sputtering with 500 eV Ar^+ and annealing to 725 K. Liquid samples of anhydrous, 99% pure $[Bmpyr]^+[NTf_2]^-$ were purchased from Sigma Aldrich. Samples were further degassed of impurities under ultrahigh vacuum conditions and elevated temperatures for 48 h prior to dosing. Ultrathin films were grown on a Ag(111) sample held at 300 K using a Knudsen cell held at 475 K.[50] Purity and molecular content of thin films were examined by standard surface science techniques including Auger spectroscopy and low energy electron diffraction (LEED). In subsequent experiments, the sample temperature was controlled within ±1 K between 130 and 350 K using a liquid nitrogen coldfinger and resistive heating.

TPPE investigations were carried out on thin films of $[Bmpyr]^+[NTf_2]^-$/Ag(111) (Figure 1a). Preliminary experiments

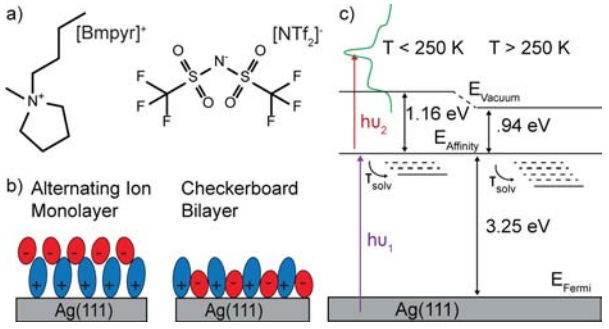

Figure 1. (a) Schematic showing chemical structures of 1-butyl-1-methylpyrrolidinium ($[Bmpyr]^+$) and bis(trifluoromethylsulfonyl) imide ($[NTf_2]^-$). (b) The growth mode is known to be either an alternating cation–anion growth mode (left) or checkerboard bilayer (right). (c) In TPPE a UV pulse excites an electron from the substrate into the EA level, and a visible pulse photoemits it to a detector. Electron solvation is observed as a dynamic decrease in the EA level. Energy of the EA level and changes in work function are measured as a function of sample temperature.

with related ionic liquids showed that sample degradation could occur under laser illumination within a few minutes. The $[Bmpyr]^+[NTf_2]^-$ degraded more slowly, over 15 min or more. In order to minimize sample degradation, all spectral acquisition times were kept shorter than 5 min, with a fluence of $<10^4$ electrons per second at the detector. The sample was moved with respect to the laser between spectra, in a raster pattern. Spectral acquisitions were randomized and repeated on freshly prepared films to ensure reproducibility.

TPPE is used in order to determine both film morphology and the kinetic response of the thin film to excess electrons. In this pump–probe spectroscopic technique, an ultraviolet pump pulse excites a charge transfer excitation from an occupied electronic state in a conductive substrate to an unoccupied state in an adsorbed film. After a variable delay time, a visible pulse photoemits an electron to a kinetic energy detector. Solvation of the intermediate state is observed as a dynamic decrease in energy (Figure 1c). In our implementation of this technique, the probe pulse ($h\upsilon_1$) is produced as the output of a visible OPA, and the pump pulse ($h\upsilon_2$) is the second harmonic of the probe. A time-of-flight detector is used to collect spectra of electron counts versus kinetic energy. With this technique, the energy of a transiently occupied electronic state can be measured relative to the Fermi and vacuum levels with a typical energy resolution of <50 meV and time resolution of <100 fs. Here, sample degredation and the resulting need for short spectral acquisition times limit achievable time resolution to 150 fs.

3. RESULTS AND DISCUSSION

3.1. Thin Film Growth Mode. The growth mode of $[Bmpyr]^+[NTf_2]^-$/Ag(111) is determined via a TPPE dosing survey (Figure 2b). In a dosing survey, $[Bmpyr]^+[NTf_2]^-$ is

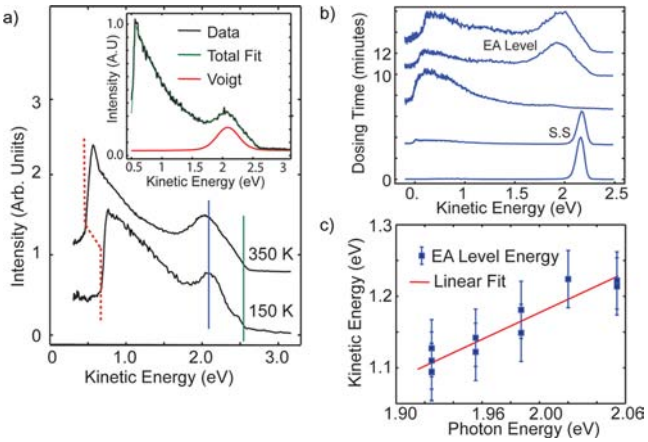

Figure 2. (a) Spectra taken at 350 and 150 K with different work functions. The Fermi level (green vertical line) and EA level (blue vertical line) are held constant by a voltage bias, while a change in surface dipole results in a shift of the low energy cutoff. Example fit is shown in the inset. (b) A dosing survey at a wavelength $h\upsilon_1$ = 630 nm shows the disappearance of the surface state (SS) of clean Ag(111) and appearance of the EA state with increasing coverage. Spectra are individually normalized to the point of maximum intensity and offset by the dosing time. (c) A wavelength survey shows the kinetic energy of the peak center versus the photon energy, $h\upsilon 1$. A slope of 0.93 ± 0.3 indicates a UV pump and visible probe.

dosed on Ag(111) at a constant rate (0.1 ML/min) and spectra are collected at increments of dosing time. Before dosing, one or two peaks are observed on clean Ag(111), corresponding to the surface state (SS) and image potential state (IPS), depending upon the pump and probe wavelengths. With increasing dosing time, a new peak appears at 3.25 ± 0.15 eV above the Fermi level, which we will identify as an electron affinity (EA) level of the RTIL adlayer, as discussed below (Figure 2b). The EA state is observed to grow in at a constant kinetic energy with increasing dosing times, indicating the growth of a single structural morphology. The IPS and SS states associated with the clean Ag(111) surface are both observed to disappear with increasing dosages. These states are sensitive to

dx.doi.org/10.1021/ja3108593 | J. Am. Chem. Soc. 2013, 135, 10646–10653

local scattering and the presence of an adsorbate, and their disappearance confirms the formation of a complete wetting layer as opposed to three-dimensional islands or droplets.[51] Further, the EA state is found to grow in at the same rate as the disappearance of the IPS and SS, indicating that this growth corresponds to a single layer of alternating cation−anion monolayer or checkerboard bilayer (Figure 1b).

The growth mode is further investigated using Auger and LEED spectroscopies. Auger spectra confirm the presence of both anion and cation species at the surface. LEED diffraction spots from the $[Bmpyr]^+[NTf_2]^-$ adlayer crystal structure are not observed, though the 6-fold symmetric spots from the Ag(111) substrate remain visible at all coverages investigated. We attribute the lack of diffraction spots from $[Bmpyr]^+[NTf_2]^-$) to degradation under the 1 μA electron beam flux. We point out that similar LEED investigations on an Au(111) substrate have also observed diffraction spots from the substrate and not the RTIL adlayer while STM images from the same study show an ordered thin film.[37] Because of the short escape depth (<1 nm) of low energy electrons, our observation of Ag(111) diffraction spots indicate a coverage of less than a few nanometers and support our assignment as a monolayer or bilayer coverage.

The work function of $[Bmpyr]^+[NTf_2]^-$/Ag(111) is measured both by the onset of one-photon photoemission and by the measured kinetic energies of the high energy and low energy cutoffs of the spectra (Figure 2a). For a work function measurement, the detector flight tube is held at an accelerating positive bias relative to the $[Bmpyr]^+[NTf_2]^-$/Ag(111) sample; change in sample work function results in an observed change in the kinetic energy of the low energy cutoff.[52] The high energy cutoff, however, corresponds to the Fermi level of the sample plus the sum of the photon energies and is held constant by the bias voltage. The high and low energy cutoffs can be used to reference intermediate states to both the Fermi and vacuum levels.

The high and low energy cutoffs of the spectra are fit to finite temperature Fermi−Dirac cutoffs, while the baseline is fit to an exponential decay from the Fermi level.[53] The work function for $[Bmpyr]^+[NTf_2]^-$/Ag(111) is measured to be 4.19 eV at 300 K, and it is found to increase to 4.41 eV near the base temperature of 130 K (Figure 2a).

This work function is larger than typically observed for dipolar solvents, alkane layers, or aromatic compounds on Ag(111). An increased work function or surface dipole results from an increase in the anionic character of the vacuum interface. In the case of RTILs, the cation component is commonly found to bind strongly to the metal substrate while the anion remains less strongly bound. Checkerboard bilayers have been commonly observed for immidizolium ionic liquids,[35,37] while stronger substrate affinity of pyrrolidinium ionic liquids in $[Bmpyr]^+[NTf_2]^-$/Au(111) has been found to favor alternating anion−cation layers.[29] Although we cannot directly distinguish between a checkerboard bilayer and alternating cation−anion morphology, the elevated work function favors the latter assignment.

3.2. Localized State Assignment and Characterization.

We observe a single electronic peak in TPPE spectra, which fits to a Voigt line shape with a typical FWHM of 400 meV (Figure 2a inset). A wavelength survey is performed in which the photon energy of the pump and probe pulses are tuned. The fit to the EA peak position (Figure 2c) has a measured slope of 0.93 ± 0.3, identifying this state as being populated by the hυ_2 and photoemitted by the hυ_1 probe. By use of the measured work function, the energy of EA is determined to be 3.25 ± 0.15 eV above the Fermi level.

Angle resolved measurements determine localization or delocalization. Momentum is conserved upon photoemission, and the EA level momentum parallel to the Ag(111) substrate can be measured as that of the photoemitted electron. A solid angle of momentum ($k_{\|}$) is detected by changing the substrate angle (θ) relative to a detector, following the dispersion relation eq 1.

$$k_{\|} = \sqrt{\frac{2m^* E_{kin}}{\hbar^2}} \sin\theta \quad (1)$$

Here E_{kin} is the measured kinetic energy and m^* is the band's effective mass relative to the mass of a free electron, m_e.[49] A large effective mass corresponds to a localized electronic state, whereas an effective mass near unity corresponds to a nearly free electron.

The EA level is found to have a flat band at all times investigated, indicating a localized state, as shown in Figure 3.

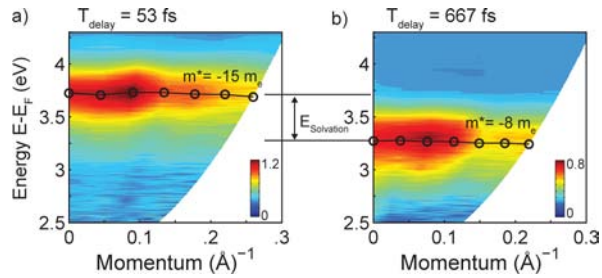

Figure 3. Angle resolved spectra at delay times of (a) 53 fs and (b) 667 fs taken at 304 K. Fits to the dispersion reveal a localized flat band at all delays. The relative population at 667 fs delay has decreased by 50%, while solvation has decreased the energy of the peak by 460 meV relative to zero time delay.

The effective mass at early time delays is found to be −15 m_e, remaining nearly constant out beyond 667 fs time delay, at which point the mass is measured to be −8 m_e. Both of these measurements are within error of a flat band (infinite effective mass). The slight negative curvature is likely a measurement artifact similar to that reported for electron solvation in ice.[42]

The observed flat dispersion of this state supports the assignment of this state as a molecularly derived EA level. Molecularly derived states in organic systems tend to be localized, in contrast to the nearly free-electron dispersions expected for image states or metal-derived surface states.

This EA state is found to decrease in intensity with increasing momentum parallel to the surface. Intensity as a function of parallel momentum can be related to the momentum-space probability density of the wave function for localized states.[53,54] Solvated and localized image states have been approximated as being localized to a Gaussian wave function, and the intensity distribution in k-space can be related to the population distribution in real space.[49] With this approximation, we can estimate the real space distribution in $[Bmpyr]^+[NTf_2]^-$ to be localized to 11 ± 5 Å, suggesting localization to one or a few ions. The intensity distribution we observe, however, has additional intensity fluctuations and does not fit well to a Gaussian. High angular resolution photoemission spectroscopy has shown that oscillations in intensity can result from the k-space distribution of a molecular wave function.[55] Improved

dx.doi.org/10.1021/ja3108593 | J. Am. Chem. Soc. 2013, 135, 10646−10653

angle resolution in future studies may allow a more detailed analysis and assignment of this peak through its intensity distribution.

3.3. Electron Population and Solvation Dynamics. The dynamic solvent response of the photoinjected electrons is measured by population and energy dynamics (Figure 4a).

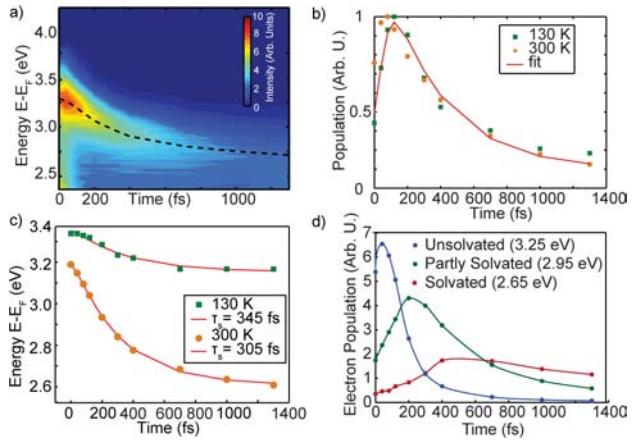

Figure 4. (a) A false color contour plot shows population and energy of the EA level as a function of time delay. (b) The rate of decay to the metal and (c) rate of solvation remain constant at low and high temperatures. (c) In contrast, the total energy of solvation is much greater at 300 K than at 130 K. (d) The population through different energy slices shows that high energy electrons decay because of both metal−molecule transfer and dynamic solvation. Population at low energy slices shows an additional rise time due to solvation from higher states.

Population decay results from decay back to the metal substrate and is a measure of molecule−metal electron transfer rates. This decay rate is found to occur on a single exponential time scale of 400 ± 150 fs, irrespective of temperature (Figure 4b).

Population decay of the electron back to the metal substrate occurs with a rate proportional to the overlap of the wave function with those of the bulk substrate.[52] This decay rate is consistent with the picture of an electron existing within a few angstroms of the substrate. The cation is known to preferentially reside at the metal interface[29] either with the anion in checkerboard monolayer[37] or at the partial or complete exclusion of the anion with alternating layer morphology.[29,30,32−34,37] Temperature independent fast decay rates favor the electron being localized in the cation. Detailed structural investigations will be required, however, to rule out possible localization on the anion in a checkerboard bilayer or localization in a state that spans both ions.

Electron solvation appears as a decrease in the peak center as a function of delay time (Figure 4c). No discrete states are observed, and we assign the decrease in peak energy to a continuous solvation mechanism. Solvation is empirically found to fit well to a single exponential decrease in energy with a time constant of 350 ± 150 fs, convoluted with the instrument response function. Although the magnitude of solvation changes dramatically as a function of temperature, the rate of solvation is found to be constant across the observed temperature range.

It is important to distinguish charge solvation from an energy dependent electron decay rate. In the case of the broad peak observed here, the high energy side could be expected to have a greater overlap with the bulk Ag sp bands, found at 4.1 eV above the Fermi level. The low energy side of the peak, however, is located in the mid-gap region between the upper and lower surface projected Ag sp bands. This could result in decreased wave function overlap with the bulk Ag and increased lifetimes on the low energy side of the peak.[52] Stahler et al. have proposed an empirical rate equation,[56] which can be used to differentiate energy-dependent electron transfer rates and solvation rate, eq 2:

$$\frac{\partial N(t,E)}{\partial t} = -N(t,E)\cdot\left(\sigma_S + \frac{1}{\tau(E)}\right) + N(t, E+\partial E)\cdot\left(\sigma_S - \frac{1}{\tau(E+\partial E)}\right) \quad (2)$$

Here, electron population, $N(t,E)$, as a function of time and energy is dependent upon both the solvation rate, σ_S, and the energy-dependent back electron transfer rate, $\tau(E)$. The population at a given energy decreases as a result of both solvation to lower energies and molecule−metal electron transfer, while population increase occurs because of solvation from higher energies, $N(t, E+\delta E)$.

In the case of ($[Bmpyr]^+[NTf_2]^-$), we examine electron population at different energy slices. The population maximum decreases from an initial peak center at 3.25 eV to a final energy of 2.65 eV over the investigated time range of 1.3 ps. We investigate the electron population dynamics at three energies showing different population dynamics (Figure 4d). The electron population at an energy of 3.25 eV is found to have a maximum population near zero time delay. This high energy portion shows an initial fast rise time within the time scale of the instrument response function, followed by a fast decay. The proceeding decay is faster than the decay of the integrated population (Figure 4d). Faster decays result from the sum of decay pathways to the metal, $N(t,E)/\tau(E)$, as well as solvation to lower energies, with a rate $N(t,E)\sigma_S$. The electron population measured at an intermediate energy 2.95 eV above the Fermi level, which represents electrons that have undergone 50% of the total solvation, shows a significant rise time, with a peak maximum 200 fs after the initial excitation. The rise time results from solvation from higher energy states, $N(t, E+\delta E)$. Finally, electron population on the low energy side of the fully solvated state, 2.65 eV, is found to increase to a maximum intensity at 500 fs, before decaying slowly. The observed decay from the low energy side of the EA level is slower because solvation to a lower energy $N(t,E)\sigma_S$ is not possible, and the only source of population decay is back to the metal. Longer decay times of the solvated electron have been used previously to determine a solvation and energy dependent trapping mechanism, slowing back electron transfer.[56] The rise times observed at the energies corresponding to partially solvated and fully solvated electrons conclusively demonstrate electron solvation in addition to possible energy-dependent decay rates to the substrate.

The decrease in energy with subpicosecond exponential kinetics allows some insight into possible mechanisms related to the energy dissipation. A trapping mechanism in which the electron diffuses to lower energy defect sites can be ruled out because the electronic state remains localized at all times. Lateral motion of a localized state on the surface would require a thermally activated hopping step, resulting in temperature-dependent solvation rates. The time scale of this solvation also rules out purely electronic effects, as these are expected to occur on a <50 fs time scale.

dx.doi.org/10.1021/ja3108593 | J. Am. Chem. Soc. 2013, 135, 10646−10653

We attribute this decrease in energy, occurring with an exponential time constant, to electron solvation in which energy is lost to the surrounding molecules.[57] Similar shifts in the energy of solvation have been observed via the dynamic Stokes shift of dye molecules in bulk solution.[14] Fits to exponential decays on different time scales or fits to multiexponential decays have been attributed to different mechanisms or different solvation environments. Solvation by diffusion of RTIL ions is generally attributed to the slower, viscosity-dependent kinetics.[58] Solvation of a localized state over a time scale of 350 fs, as we observe in our results, may be due to the inertial response[58] of the solvent or polarization response within the cation[16] or cation alkyl chain.[20] In cases where biexponential decay has been observed, energy dissipation on two time scales has been attributed to two separate populations with different local morphologies. Electron solvation kinetics at the $[Bmpyr]^+[NTf_2]^-$/Ag(111) interface are comparable to the fastest time scales observed in bulk ionic liquids. It is possible that we only observe a single time scale because the electron is localized in only a single chemical environment, or it is possible that a slower component of solvation is unobserved because of competitive fast decay to the metal substrate. We observe a strong solvation with a subpicosecond time constant while no slower time constants are observed, suggesting that a single morphology and mechanism may dominate electron solvation at the interface.

3.4. Characterization of High and Low Temperature Regimes. A temperature dependent work function shift reveals a morphological transition in $[Bmpyr]^+[NTf_2]^-$/Ag(111) as measured via the high and low energy cutoffs (Figure 2a).[48] The low energy cutoff increases in kinetic energy by 245 ± 80 meV as the substrate is cooled from 350 to 130 K (Figure 5a) as a result of a change in the surface dipole.

The change in work function ($\Delta\Phi$) or surface dipole in a molecular thin film is often attributed to a reorientation of molecular dipoles (P), eq 3:

$$\Delta\Phi = \frac{e}{\varepsilon_0} P \frac{\theta}{d^2} \tag{3}$$

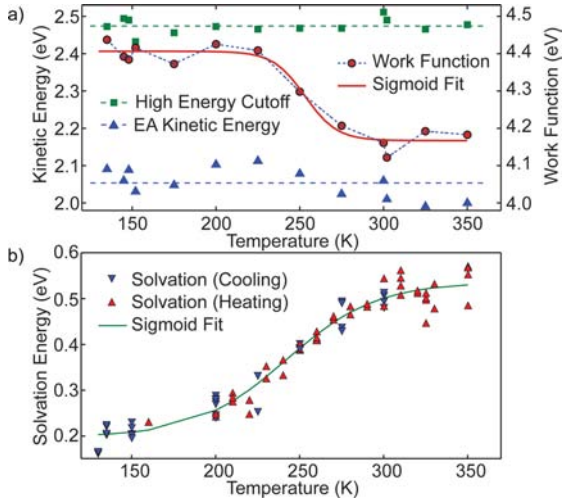

Figure 5. A morphological transition is observed by the temperature dependence of (a) the work function and (b) magnitude of solvation, as measured by $E(t=0) - E(t=1.3\ ps)$. No hysteresis is observed in the solvation energy upon heating versus cooling within experimental error.

where ε_0 is the vacuum permittivity, P is the molecular dipole, and θ is the number of molecules per d^2 area of a molecule.[59] An approximate unit cell size per cation−anion pair 6 Å on a side can be estimated from the known bulk crystal structure[60] or from measured surface unit cells.[29] With the measured work function change, this equation estimates the change in surface-normal projected dipole to be 0.2 D. If the change in work function were due solely to a reorientation of a single ion, a rotation of either the anion, with dipole 0.6 D,[61] or cation, with dipole 3.9 D, would be adequate to account for this change.

For ionic liquids, however, collective reorientation of the anion and cation contributes to a work function shift, even in the case of a cation statically bound to the substrate. Although a specifically dipolar description of the cation and anion is inadequate for ionic liquids, ordering of anions relative to the cations results in a collectively defined surface dipole. A collective reorientation, such as a softening of the cation layer and movement of the anion toward the Ag(111) substrate, could be invoked to explain the lower work function occurring in the high temperature regime.

Morphology dependent work function has been observed in adsorbed immidazolium chloride ionic liquids on patterned substrates.[62] Zhang et al. used a kelvin probe to measure the surface dipole, which is found to depend upon the molecular orientation of the ionic liquid adsorbates on chemically different substrates. Molecular rearrangements have been observed in both temperature- and voltage-dependent studies at RTIL interfaces. A voltage-dependent change in X-ray reflectivity was observed in $[Bmpyr]^+[NTf_2]^-$/Au.[29] This study found that the Au interface remained cation-rich at all voltages, while the vacuum interface was anion-rich at positive voltages and mixed character at negative voltages. Orientation changes have been observed in imidazolium ionic liquids at a metal interface as a function of temperature[63] and voltage.[64] Further work will be necessary to distinguish the relative importance of anion and cation rotations or translations in surface reordering and the effects on the surface dipole.

In order to understand the low and high temperature regimes, we compare our results to a model for a thermally activated phase transition of a two-phase material at equilibrium. Spectroscopic investigations of equilibrium phase transitions can be fit to a Boltzmann sigmoid.[65−67] This results from modeling a spectroscopic observable (Φ) of the partition function for a two-state molecular system, eq 4:

$$\Phi(T) = \frac{\Phi_A}{1 + e^{(T-T_0)/D}} + \frac{\Phi_B}{1 + e^{-(T-T_0)/D}} \tag{4}$$

Here T is the sample temperature and T_0 is the transition temperature. The variable D defines the width of the transition and is a derived as a measure of the enthalpy of the morphological transition and the size of molecular clusters. In this investigation, Φ_A and Φ_B are the work functions of the low temperature and high temperature regimes, and $\Phi(T)$ is the measured work function of the sample. Phase coexistence is expected to result in a continuous shift in work function here because regions with character of the low and high temperature regimes will both contribute to the global work function. The measured work function in Figure 5a is fit to a Boltzmann sigmoidal, with a transition temperature of T_0 = 253 ± 16 K and a broadening parameter D = 13 ± 6 K. The high and low temperature limits of the work function are found to be 4.41 eV at 130 K and 4.19 eV at 350 K.

dx.doi.org/10.1021/ja3108593 | J. Am. Chem. Soc. 2013, 135, 10646−10653

The total change in electronic energy upon solvation also shows different high and low temperature regimes. This reorganizational energy is measured by subtracting the final energy of the peak center from the initial energy at zero delay. The EA level solvates by 540 ± 40 meV at 350 K, while it solvates by only 200 ± 40 meV at 130 K. Total energy of solvation versus sample temperature is fit to eq 4 with T_0 = 242 ± 10 K and D = 25 ± 10 K (Figure 5a). The T_0 measured by electron solvation magnitude matches that of the temperature-dependent work function within error bars, which are reported as 95% confidence interval.[68]

Although we can assign a critical temperature, a simple fit such as this does not characterize thermodynamic parameters. Assigning phases or phase transitions is often complex as, for example, even relatively simple order−disorder phase transitions can be either first order or second order depending upon accompanying structural changes.[69,70] A first-order phase transition has a discontinuity in the free energy at the critical temperature, and phase transitions can often be observed through hysteresis in the critical temperature upon heating and cooling.[71] This hysteresis results from the presence of metastable states with long equilibration times and results in the observation of different ratios of the high temperature and low temperatures states upon heating or cooling.[72]

We investigated the possibility of a first-order phase transition by measuring the electron solvation magnitude upon heating versus cooling the sample. Although not a direct thermodynamic parameter, this value was found to be the most sensitive measure of the low and high temperature regimes. The results of 93 separate fits to the solvation magnitude, approximated here as the difference in the energy of the peak center measured in zero time delay spectrum and at a time delay of 1.3 ps, were used to examine possible hysteresis (Figure 5b). No thermal hysteresis is observed, and we are not able to assign a thermodynamic mechanism to the temperature dependence. Interestingly, however, the high and low temperature regimes of the work function and energy of solvation occur at about the same critical temperature, and it is likely that the high and low temperature regimes in solvation and work function result from a common microscopic mechanism.

The difference in energy of solvation between the low and high temperature phases may be due to a change in deformability.[49] As discussed in the section Introduction and Background, electron solvation in ultrathin films is dependent upon surface ordering and the deformability of molecules, particularly in amorphous systems or near step edges. Solvation magnitude may be due to two different degrees of deformability above and below the critical temperature.

4. CONCLUSIONS

We have observed charge injection and dynamic electron solvation at the $[Bmpyr]^+[NTf_2]^-$/Ag(111) interface. This interface is shown to form a wetting layer or surface filling alternating monolayer, as identified by TPPE and supported by LEED and Auger spectroscopies. A single charge-injection state is observed between the Fermi and vacuum levels of the sample, which is identified as a localized electronic state, using angle- and time-resolved measurements.

A single temperature-dependent morphological transition is responsible for both a change in work function and a change in the reorganizational energy associated with dynamic solvation of a localized state. An increase in work function at 130 K relative to 350 K results from relative reorientations of the ions; the increase in surface dipole results from an increase in the amount of negative charge on the vacuum side of the interface. Solvent responses in the high and low temperature limits show nearly identical kinetics, though a dramatically different magnitude, which may result from a change in the relative deformability of the sample.

Injected interfacial electrons are observed to solvate with an ultrafast time scale of 350 fs. This observation is striking in contrast to common measurements of slow kinetics in bulk RTIL. Further investigation will be required to assign this ultrafast solvation to a specific molecular mechanism. We expect these results to be general and applicable toward an understanding of the molecular mechanisms governing electronic and electrochemical devices that depend upon reorientation dynamics at the interface.

AUTHOR INFORMATION

Corresponding Author

*cbharris@berkeley.edu

Notes

The authors declare no competing financial interest.

ACKNOWLEDGMENTS

This work was supported by the Director, Office of Science, Office of Basic Energy Sciences, Chemical Sciences Division of the U.S. Department of Energy under Contract No. DE-AC02-05CH11231. We acknowledge NSF support for specialized equipment used in the experiments herein.

REFERENCES

(1) Earle, M.; Seddon, K. *Pure Appl. Chem.* **2000**, *72*, 1391.
(2) Mehnert, C.; Cook, R.; Dispenziere, N.; Afeworki, M. *J. Am. Chem. Soc.* **2002**, *124*, 12932.
(3) Wang, P.; Zakeeruddin, S.; Comte, P.; Exnar, I.; Gratzel, M. *J. Am. Chem. Soc.* **2003**, *125*, 1166.
(4) Lewandowski, A.; Swiderska-Mocek, A. *J. Power Sources* **2009**, *194*, 601.
(5) Matsumoto, H.; Sakaebe, H.; Tatsumi, K.; Kikuta, M.; Ishiko, E.; Kono, M. *J. Power Sources* **2006**, *160*, 1308.
(6) Angell, C. A.; Ansari, Y.; Zhao, Z. F. *Faraday Discuss.* **2012**, *154*, 9.
(7) Zhou, Z.; Matsumoto, H.; Tatsumi, K. *Chem.—Eur. J.* **2004**, *10*, 6581.
(8) Wang, H.; Liu, S.; KelongHuang; Yin, X.; Liu, Y.; Peng, S. *Int. J. Electrochem. Sci.* **2012**, *7*, 1688.
(9) Zhou, Q.; Boyle, P.; Malpezzi, L.; Mele, A.; Shin, J.; Passerini, S.; Henderson, W. *Chem. Mater.* **2011**, *23*, 4331.
(10) Zhao, X.; Sanchez, B.; Dobson, P.; Grant, P. *Nanoscale* **2011**, *3*, 839.
(11) Fee, R. S.; Maroncelli, M. *Chem. Phys.* **1994**, *183*, 235.
(12) Shirota, H.; Funston, A.; Wishart, J.; Castner, E. *J. Chem. Phys.* **2005**, 122.
(13) Castner, E.; Wishart, J.; Shirota, H. *Acc. Chem. Res.* **2007**, *40*, 1217.
(14) Maroncelli, M.; Zhang, X.; Liang, M.; Roy, D.; Ernsting, N. *Faraday Discuss.* **2012**, *154*, 409.
(15) Weingartner, H.; Sasisanker, P.; Daguenet, C.; Dyson, P.; Krossing, I.; Slattery, J.; Schubert, T. *J. Phys Chem. B* **2007**, *111*, 4775.
(16) Chowdhury, P.; Halder, M.; Sanders, L.; Calhoun, T.; Anderson, J.; Armstrong, D.; Song, X.; Petrich, J. *J. Phys. Chem. B* **2004**, *108*, 10245.
(17) Fruchey, K.; Lawler, C. M.; Fayer, M. D. *J. Phys. Chem. B* **2012**, *116*, 3054.
(18) Patra, S.; Samanta, A. *J. Phys. Chem. B* **2012**, *116*, 12275.
(19) Cang, H.; Li, J.; Fayer, M. D. *J. Chem. Phys.* **2003**, *119*, 13017.
(20) Fruchey, K.; Fayer, M. D. *J. Phys. Chem. B* **2010**, *114*, 2840.

(21) Li, J.; Wang, I.; Fruchey, K.; Fayer, M. D. *J. Phys. Chem. A* **2006**, *110*, 10384.
(22) Shkrob, I. A.; Wishart, J. F. *J. Phys. Chem. B* **2009**, *113*, 5582.
(23) Wishart, J. F.; Funston, A. M.; Szreder, T.; Cook, A. R.; Gohdo, M. *Faraday Discuss.* **2012**, *154*, 353.
(24) Margulis, C.; Annapureddy, H.; De Biase, P.; Coker, D.; Kohanoff, J.; Del Popolo, M. *J. Am. Chem. Soc.* **2011**, *133*, 20186.
(25) Lisal, M.; Posel, Z.; Izak, P. *Phys. Chem. Chem. Phys.* **2012**, *14*, 5164.
(26) Men, S.; Hurisso, B.; Lovelock, K.; Licence, P. *Phys. Chem. Chem. Phys.* **2012**, *14*, 5229.
(27) Baldelli, S. *J. Phys. Chem. Lett.* **2012**, *4*, 244.
(28) Lockett, V.; Sedev, R.; Harmer, S.; Ralston, J.; Horne, M.; Rodopoulos, T. *Phys. Chem. Chem. Phys.* **2010**, *12*, 13816.
(29) Lauw, Y.; Horne, M.; Rodopoulos, T.; Lockett, V.; Akgun, B.; Hamilton, W.; Nelson, A. *Langmuir* **2012**, *28*, 7374.
(30) Carstens, T.; Hayes, R.; El Abedin, S. Z.; Corr, B.; Webber, G. B.; Borisenko, N.; Atkin, R.; Endres, F. *Electrochim. Acta* **2012**, *82*, 48.
(31) Lynden-Bell, R. M.; Frolov, A. I.; Fedorov, M. V. *Phys. Chem. Chem. Phys.* **2012**, *14*, 2693.
(32) Hayes, R.; Borisenko, N.; Tam, M.; Howlett, P.; Endres, F.; Atkin, R. *J. Phys. Chem. C* **2011**, *115*, 6855.
(33) Atkin, R.; Borisenko, N.; Druschler, M.; El Abedin, S. Z.; Endres, F.; Hayes, R.; Huber, B.; Roling, B. *Phys. Chem. Chem. Phys.* **2011**, *13*, 6849.
(34) Atkin, R.; El Abedin, S.; Hayes, R.; Gasparotto, L.; Borisenko, N.; Endres, F. *J. Phys. Chem. C* **2009**, *113*, 13266.
(35) Foulston, R.; Gangopadhyay, S.; Chiutu, C.; Moriarty, P.; Jones, R. *Phys. Chem. Chem. Phys.* **2012**, *14*, 6054.
(36) Krischok, S.; Eremtchenko, M.; Himmerlich, M.; Lorenz, P.; Uhlig, J.; Neumann, A.; Ottking, R.; Beenken, W.; Hofft, O.; Bahr, S.; Kempter, V.; Schaefer, J. *J. Phys. Chem. B* **2007**, *111*, 4801.
(37) Cremer, T.; Stark, M.; Deyko, A.; Steinruck, H.; Maier, F. *Langmuir* **2011**, *27*, 3662.
(38) Smith, A. M.; Lovelock, K. R. J.; Gosvami, N. N.; Licence, P.; Dolan, A.; Welton, T.; Perkin, S. *J. Phys. Chem. Lett.* **2013**, *4*, 378.
(39) Drueschler, M.; Borisenko, N.; Wallauer, J.; Winter, C.; Huber, B.; Endres, F.; Roling, B. *Phys. Chem. Chem. Phys.* **2012**, *14*, 5090.
(40) Pinilla, C.; Del Popolo, M.; Kohanoff, J.; Lynden-Bell, R. *J. Phys. Chem. B* **2007**, *111*, 4877.
(41) Bovensiepen, U.; Gahl, C.; Stahler, J.; Loukakos, P.; Wolf, M. *Isr. J. Chem.* **2005**, *45*, 171.
(42) Bovensiepen, U.; Gahl, C.; Wolf, M. *J. Phys. Chem. B* **2003**, *107*, 8706.
(43) Stahler, J.; Mehlhorn, M.; Bovensiepen, U.; Meyer, M.; Kusmierek, D.; Morgenstern, K.; Wolf, M. *Phys. Rev. Lett.* **2007**, *98*, 206105.
(44) Meyer, M.; Stahler, J.; Kusmierek, D.; Wolf, M.; Bovensiepen, U. *Phys. Chem. Chem. Phys.* **2008**, *10*, 4932.
(45) Onda, K.; Li, B.; Zhao, J.; Jordan, K.; Yang, J.; Petek, H. *Science* **2005**, *308*, 1154.
(46) Onda, K.; Li, B.; Zhao, J.; Petek, H. *Surf. Sci.* **2005**, *593*, 32.
(47) Li, B.; Zhao, J.; Onda, K.; Jordan, K.; Yang, J.; Petek, H. *Science* **2006**, *311*, 1436.
(48) Liu, S.; Miller, A.; Gaffney, K.; Szymanski, P.; Garrett-Roe, S.; Bezel, I.; Harris, C. *J. Phys. Chem. B* **2002**, *106*, 12908.
(49) Strader, M.; Garrett-Roe, S.; Szymanski, P.; Shipman, S.; Johns, J.; Yang, A.; Muller, E.; Harris, C. *J. Phys. Chem. C* **2008**, *112*, 6880.
(50) Zaitsau, D.; Kabo, G.; Strechan, A.; Paulechka, Y.; Tschersich, A.; Verevkin, S.; Heintz, A. *J. Phys. Chem. A* **2006**, *110*, 7303.
(51) Yang, A.; Shipman, S.; Garrett-Roe, S.; Johns, J.; Strader, M.; Szymanski, P.; Muller, E.; Harris, C. *J. Phys. Chem. C* **2008**, *112*, 2506.
(52) Fauster, T.; Steinmann, W. In *Electromagnetic Waves: Recent Developments in Research*; Halevi, P., Ed.; Elsevier: Amsterdam, 1994; Vol. 2, p 347.
(53) Muller, E.; Johns, J.; Caplins, B.; Harris, C. *Phys. Rev. B* **2011**, *83*, 165422.
(54) Mugarza, A.; Mascaraque, A.; Repain, V.; Rousset, S.; Altmann, K. N.; Himpsel, F. J.; Koroteev, Y. M.; Chulkov, E. V.; de Abajo, F. J. G.; Ortega, J. E. *Phys. Rev. B* **2002**, 66.
(55) Puschnig, P.; Berkebile, S.; Fleming, A. J.; Koller, G.; Emtsev, K.; Seyller, T.; Riley, J. D.; Ambrosch-Draxl, C.; Netzer, F. P.; Ramsey, M. G. *Science* **2009**, *326*, 702.
(56) Stahler, J.; Gahl, C.; Bovensiepen, U.; Wolf, M. *J. Phys. Chem. B* **2006**, *110*, 9637.
(57) Chernyak, V.; Mukamel, S. *J. Chem. Phys.* **2001**, *114*, 10430.
(58) Arzhantsev, S.; Jin, H.; Baker, G.; Maroncelli, M. *J. Phys. Chem. B* **2007**, *111*, 4978.
(59) Gensterblum, G. H., K.; Han, B.; Yu, L.; Pireaux, J.; Thiry, P.; Caudano, R.; Lucas, A.; Bernaerts, D.; Amelinckx, S.; Vantendeloo, G.; Bendele, G.; Buslaps, T.; Johnson, R.; Foss, M.; Feidenhansl, R.; Lelay, G. *Phys. Rev. B* **1994**, *50*, 11981.
(60) Choudhury, A.; Winterton, N.; Steiner, A.; Cooper, A.; Johnson, K. *J. Am. Chem. Soc.* **2005**, *127*, 16792.
(61) Kobrak, M.; Li, H. *Phys. Chem. Chem. Phys.* **2010**, *12*, 1922.
(62) Zhang, X.; Lu, L.; Cai, Y. *Langmuir* **2012**, *28*, 9593.
(63) Krischok, S.; Eremtchenko, M.; Himmerlich, M.; Lorenz, P.; Uhlig, J.; Neumann, A.; Ottking, R.; Beenken, W.; Hofft, O.; Bahr, S.; Kempter, V.; Schaefer, J. *J. Phys. Chem. B* **2007**, *111*, 4801.
(64) Baldelli, S. *Acc. Chem. Res.* **2008**, *41*, 421.
(65) Kirchhoff, W.; Levin, I. *J. Res. Natl. Bur. Stand.* **1987**, *92*, 113.
(66) Marks, M.; Schmidt, C.; Schwalb, C.; Breuer, T.; Witte, G.; Hofer, U. *J. Phys. Chem. C* **2012**, *116*, 1904.
(67) Douglas, J.; Dudowicz, J.; Freed, K. *J. Chem. Phys.* **2008**, *128*, 224901.
(68) Alper, J.; Gelb, R. *J. Phys. Chem.* **1990**, *94*, 4747.
(69) Golosov, N. S.; Tolstik, A. M. *J. Phys. Chem. Solids* **1975**, *36*, 903.
(70) Mecke, K. R.; Dietrich, S. *Phys. Rev. B* **1995**, *52*, 2107.
(71) Efremov, M.; Olson, E.; Zhang, M.; Zhang, Z.; Allen, L. *Macromolecules* **2004**, *37*, 4607.
(72) Agarwal, G.; Shenoy, S. *Phys. Rev. A* **1981**, *23*, 2719.